Check for updates

View Article Online
View Journal

NJC

Accepted Manuscript

This article can be cited before page numbers have been issued, to do this please use: M. Kondeboina, S. Enumula, V. R. B. Gurram, J. Yadagiri, D. R. Burri and K. S. Rama Rao, *New J. Chem.*, 2018, DOI: 10.1039/C8NJ03211D.

ROYAL SOCIETY
OF CHEMISTRY

rsc.li/njc

View Article Online
DOI: 10.1039/C8NJ03211D

Journal Name

ARTICLE

Received 00th January 20xx,

Accepted 00th January 20xx

DOI: 10.1039/x0xx00000x

www.rsc.org/

Mesoporous silica supported cobalt catalysts for gas phase hydrogenation of Nitrobenzene: Role of pore structure on stable catalytic performance

Murali Kondeboina,[a] Siva Sankar Enumula,*[a] Venkata Ramesh Babu Gurram,[a] Jyothi Yadagiri,[a] David Raju Burri,[a] Seetha Rama Rao Kamaraju*[a]

Highly dispersed cobalt nanoparticles were prepared over mesoporous silica with different pore structures (2D-hexagonal COK-12 and 3D- cubic SBA-16). These catalysts were evaluated for gas phase hydrogenation of nitrobenzene to aniline at atmospheric H_2 pressure. A combination of catalytic activity and characterization results were assessed to establish the role of support pore structure on hydrogenation activity. XRD, N_2-physisorption, SEM and TEM analysis confirmed the presence of mesoporous structures in the supported cobalt catalysts. H_2-TPR, H_2-pulse chemisorption and TEM studies demonstrated higher dispersion of cobalt nanoparticles in Co/SBA-16 than Co/COK-12 catalyst. During time-on-stream study Co/SBA-16 catalyst experienced a gradual deactivation where as Co/COK-12 catalyst exhibited constant catalytic performance in hydrogenation of nitrobenzene. 3D-SBA-16 support with interconnected cage type pores facilitated the product to diffuse and readsorb possibly on a cobalt particle to another partilce. It resluted the formation of condensed products and coke deposition. Co/SBA-16 catalyst was rapidily deactivated due to pore blocking through coke deposition. N_2-physisorption, TGA, H_2-TPR and CHNS elemental analysis of spent catalysts confirmed the severe coke deposition in Co/SBA-16 catalyst than Co/COK-12 catalyst.

Introduction

Hydrogenation of nitrobenzene (NB) to aniline (AL) is an industrially interested reaction from its inception because the product AL has been associated with global economical interests [1]. AL is the commodity chemical for rubber, plastics, herbicides, dyes and pigment industries. AL is found to be the raw material in synthesis of polyurethane foam [2-3]. The conventional procedure for synthesis of AL is hydrogenation of NB over supported metal catalysts. Pt/C [4], Pt/Carbon nanotubes [5], Pd-B/SiO_2 [6], Pd/ Mg-Al oxide hydrotalcite [7], Pd/C [8], Ru/Al_2O_3 and Ru/SiO_2 [9], Ru/C [10] catalysts have been investigated and optimized for the hydrogenation of NB. Apart from noble metal catalysts, other supported metal catalysts such as supported Ni and supported Cu have also been studied [11-12]. However, there are complications to be eliminated for their practical applications. In supported metal catalysts, nature of support plays a vital role in dispersing and stabilizing the metal particles. In view of dispersion and stabilization of metal particles, mesoporous silica's are one of the finest supports for dispersing metal particles over their high surface areas through their uniform pore channels. H_2O molecules are released during the hydrogenation of NB so that the support material has to be water resistant. In this regard, the hydrophobic nature of mesoporous silica is helpful for maintaining support stability [13-14]. Chary et al. reported Ru/SBA-15 catalyst for hydrogenation of NB at 548 K in continuous process [9]. Cheng et al. developed Pt-Pd bimetallic nanoparticles supported on an imine functionalized SBA-15 for hydrogenation of NB in batch process [15]. Huiping et al. synthesized spherical-like Pt–MCM-41 catalysts in one pot synthesis method and subjected to the hydrogenation of NB. The catalytic performance of spherical-like Pt–MCM-41 catalyst was much better than the conventional Pt/MCM-41 catalyst [16]. Viswanathan et al. studied role of Au in hydrogenation activity of Co loaded SBA-15 catalysts. Even 1 wt% Au had enormously increased the catalytic performance of Co loaded SBA-15 in hydrogenation of NB [17]. Recently, Jamileh et al. has reported enhanced catalytic activity of mesoporous silica supported cobalt catalysts in oxidation of Cyclohexanol to Cyclohexanone [18]. The key role of mesoporous silica as support for cobalt nanoparticles is illustrated in hydrogenation of furfural to furfuryl alcohol. Co/SBA-15 catalyst possesses high dispersion of cobalt nanoparticles. Its recyclability demonstrates the metal support interaction between cobalt nanoparticles and SBA-15 [19]. Even though the mesoporous silica's are better supports, their pore architectures are also important in determining the

---

[a] *Catalysis and Fine Chemicals Division, CSIR-Indian Institute of Chemical Technology, Hyderabad, India-500 007, E-mail: ksramaraoiict@gmail.com, sivasankar.enumula@gmail.com Fax: +91-40-27160921, Tel: +91-40-27193163.*

View Article Online
DOI: 10.1039/C8NJ03211D

catalytic activity. On continuation of our research work on developing active and selective stable catalytic system for the hydrogenation of NB, herein an attempt has been made to optimize a mesoporous silica (2D-hexagonal COK-12) supported cobalt catalyst for hydrogenation of NB under mild reaction conditions in continuous process. Among the series of Co/COK-12 catalysts, 5 wt% Co/COK-12 has demonstrated the best results. Hence, a further investigation has been made on 5 wt% Co/3D-cubic SBA-16 catalyst to understand role of support pore structure in supported cobalt catalysts. In order to achieve the best yields, various reaction parameters have been optimized and correlated with characterization results.

Experimental

Preparation of COK-12

Mesoporous silica, COK-12 (2 Dimensional hexagonal) was prepared by self-assembly method as reported in literature [20]. In a typical synthesis, COK-12 was prepared by dissolving 20.0 g of triblock co-polymer Pluronic, P123 (M/s Sigma Aldrich, USA) in 550 g water. To this solution, 18.42 g of citric acid monohydrate (M/s.SD Fine Chem. Ltd., India) and 12.7 g trisodium citrate (M/s. SD Fine Chem. Ltd., India) were added. The resulting solution was stirred for 24 h. 52 g sodium silicate solution was diluted (M/s. Merck, Germany) in 150 g of water and added to the solution containing P123 and citric acid. The resultant solution was stirred for 5 min at 175 rpm and kept at room temperature without agitation for 24 h. The synthesized material was filtered, washed and dried at 373 K for 12 h. Finally the material was calcined in air in two steps, 8 h at 573 K followed by 8 h at 823 K with 1 K min^{-1} ramp. The obtained solid was used as support for the catalysts preparation.

Preparation of SBA-16

SBA-16 (3 Dimensional cubic) was prepared according to literature described elsewhere by using triblock copolymer surfactant ($EO_{106}PO_{70}EO_{106}$, called F127 (M/s. Sigma Aldrich chemicals, USA)) as a structure directing agent and tetraethyl orthosilicate (TEOS, M/s. Sigma-Aldrich chemicals, USA) as silica source [21]. In a typical synthesis, 17.68 g of F127 was dissolved in 661.02 ml 0.5 M HCl at 313 K. After 3h stirring, 85.71 mL of TEOS was added drop by drop. The solution containing molar composition 1 TEOS: 0.00367 F127: 0.864 HCl: $100.231H_2O$ was stirred for 20 h at 313 K, and subsequently transferred to Teflon bottle and aged at autogenous pressure for 24 h at 373 K. The material was filtered with several washings by using deionised water and dried at 373 K, and then calcined at 823 K for 6 h with a heating rate of 3 K min^{-1} in air flow. The obtained solid was used as support for the catalysts preparation.

Preparation of supported COK-12 and SBA-16 cobalt catalysts

Various Co loaded (3, 5, 10 and 20 wt %) Co/COK-12 catalysts were prepared by wet-impregnation method with Co $(NO_3)_2.6H_2O$ as Co precursor. In a typical synthesis the requisite amount of Co precursor was dissolved in water, to this solution COK-12 was added and heated on a hot plate at 353 K and kept in oven at 373 K for 12 h. It was calcined in static air at 773 K for 5 h. In similar fashion, 5wt% cobalt on SBA-16 was also prepared. The samples were labelled as 3CC-12, 5CC-12, 10CC-12 and 20CC-12 for Co/COK-12 and 5CS-16 for Co/SBA-16 catalysts respectively. The spent catalysts 5CC-12 and 5CS-16 were designated as U5CC-12 and U5CS-16 respectively.

Characterization of catalysts

X-ray diffraction patterns of all the catalysts were obtained on an Ultima-IV (M/s. Rigaku Corporation, Japan) XRD unit and it is operated at 40 kV and 40 mA equipped with nickel-filtered Cu K_α radiation (λ = 1.54056 Å) and a 2θ value ranging from 0.7 to 80° at a scanning rate of 0.5 degree/min. BET specific surface areas, pore volumes and pore sizes was determined by using the N_2 physisorption studies (M/s. Quantachrome Instruments, USA) by nitrogen adsorption at 77 K. Prior to measurement, the samples were degassed at 423 K for 2 h. The morphological studies of catalysts were carried out by scanning electron microscope (M/s. JEOL, Switzerland) and TEM images were obtained on a JEM 2000EXII apparatus (M/s. JEOL, Switzerland) operating between 160 and 180 kV respectively. Prior to TEM analysis, the catalyst sample was ultrasonicated in ethanol and a drop was placed onto a carbon coated copper grid, the solvent was then evaporated in an air oven at 353 K for 6 hours. Temperature programmed reduction (TPR) was performed in a laboratory-built equipment containing a quartz reactor with electrical heating and gas chromatograph equipped thermal conductivity detector (TCD). About 100 mg of catalyst placed at the centre of the quartz reactor between two plugs of quartz wool was pre-treated at 573 K for 1 h in Ar flow (60 ml min^{-1}). Then the catalyst was exposed to 5% H_2 balance Ar gas flow for 1 h at 373 K followed by raising the temperature of sample up to 1123 K at a heating rate of 10 K min^{-1}. FT–IR patterns were recorded on a spectrum GX spectrometer (M/s. Perkin-Elmer, Germany) in the scan range of 4000–400 cm^{-1}. H_2-Pulse chemisorption studies were carried out on automated gas sorption analyzer AUTOSORB-iQ (M/s. Quanta chrome Instruments, USA) to determine dispersion, particle size and metal surface area of catalysts. Prior to adsorption measurements 100 mg catalyst was reduced at 773 K for 3 h followed evacuation for another 1 h to remove adsorbed hydrogen on surface of the catalysts. The sample was cooled to ambient temperature (313 K) and at this temperature H_2 uptake was determined by giving H_2 (100μl) pulses subsequently. From these results the monolayer uptake (Nm), active metal surface area (AMSA), metal dispersion (D) and particle size (d) were calculated by using TPRWin software. The actual weight of cobalt was calculated by means of ICP-OES

View Article Online
DOI: 10.1039/C8NJ03211D

(M/s. Thermo Scientific iCAP6500 DU) by dissolving the sample in the aquaregia. (a few drops of hydrofluoric acid added). The Wight percentage of carbon deposition on surface of catalysts was analyzed by CHNS elemental analysis and TGA technique (TGA Q-500).

Activity test

The catalyst was packed at the centre of reactor between two plugs of quartz wool and quartz beads were placed above the catalyst bed to act as a preheating zone. Prior to the reaction the catalyst was reduced at 773 K for 4 h with H_2 flow rate of 40 mL/min. The temperature was cool down to 488 K where NB was fed at flow rate 1 mL/h by using a syringe feed pump (M/s. B. Braun, Germany) with H_2/NB mole ratio of 4. Unless otherwise specified the reaction conditions are same. The product mixture was collected in an ice cooled trap at the regular intervals and analyzed by a FID equipped gas chromatograph, GC-17A (M/s. Shimadzu Instruments, Japan) and confirmed by GC-MS, QP-2010 (M/s. Shimadzu Instruments, Japan).

$$\textbf{Conversion of NB} = \frac{\textbf{NB}_{\textbf{in}} - \textbf{NB}_{\textbf{out}}}{\textbf{NB}_{\textbf{in}}} \times \textbf{100}$$

$$\textbf{Selectivity to AL}\ (\%) = \frac{\textbf{AL formed}}{\textbf{Sum of all the products}}\ \textbf{x 100}$$

$$\textbf{Yield} = \frac{\textbf{Conversion of NB} \times \textbf{Selectivity to AL}}{\textbf{100}}$$

$$\textbf{Rate r}_{\textbf{AL}} = \frac{\textbf{Yield of AL} \times \textbf{NB}_{\textbf{feed rate}}\ (\mu\textbf{mol. s}^{-1})}{\textbf{Weight of catalyst}\ (\textbf{g}_{\textbf{cat}})}$$

$$\textbf{Turn Over Frequency (TOF)} = \frac{\textbf{Rate r}_{\textbf{AL}}\ (\mu\textbf{mol.g}^{-1}.\textbf{s}^{-1})}{\textbf{H}_2\ \textbf{uptake}\ \ (\mu\textbf{mol.g}^{-1})}$$

Results and Discussion

Fig.1 displays the low angle XRD patterns of pristine COK-12, SBA-16 and their supported cobalt catalysts. From the low angle XRD patterns it can be observed that the parent COK-12 and Co/COK-12 catalysts retained their mesoporous structural integrity by exhibiting three well resolved diffraction peaks at 2θ values of 1.02, 1.7 and 2.0˚ representing (100), (110) and (200) planes respectively of regular mesoporous 2D hexagonal pore (p6mm) structure [20]. The intensity of (100) reflection is decreasing with increase in cobalt loading. This phenomenon might be due to the partial loss of structural order or the reduced scatter contrasts between the pores and walls after loading metal particles in the pore channels of mesoporous silica [22]. The parent SBA-16 and 5CS-16 catalysts show well resolved diffraction peaks at 2θ values of 0.88, 1.01 and 1.4˚ corresponding to (110), (200) and (211) planes respectively of regular mesoporous 3D cubic pore (Im3m) structure [23,24]. The wide angle XRD patterns of calcined sample of Co/COK-12 and 5CS-16 were presented in Fig.2. The broad peak at around 2θ value of 22° corresponds to amorphous silica [22]. The XRD patterns of all Co/COK-12 and 5CS-16 catalysts show peaks at around 2θ values of 31.2, 36.8, 44.8, 59.3 and 65.2° which confirm the existence of crystalline spinel of Co_3O_4 with space group Fd3m (JCPDF 781970). 3CC-12 catalyst exhibits low intense diffraction peaks due to high dispersion of cobalt. The formation of bigger cobalt oxide crystallites is illustrated by the increase in crystallite sizes of Co_3O_4 with cobalt loading. Compared to 5CC-12 catalyst 5CS-16 catalyst shows lesser intense peaks due to high dispersion of cobalt on 3D-cubic SBA-16 support.

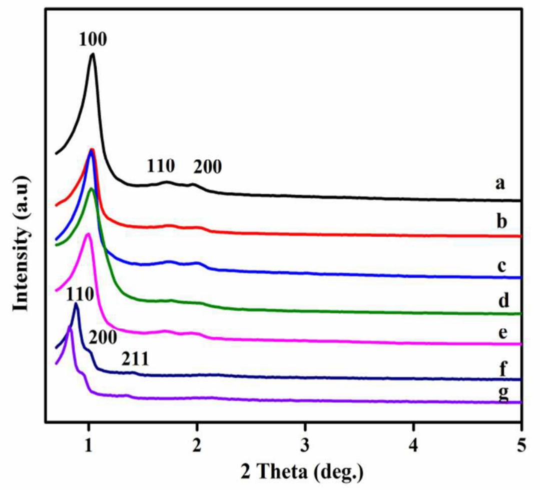

Fig. 1 Low angle XRD patterns of pristine COK-12, SBA-16 and their supported cobalt catalysts, (a) COK-12 (b) 3CC-12 (c) 5CC-12 (d) 10CC-12 (e) 20CC-12 (f) SBA-16 (g) 5CS-16

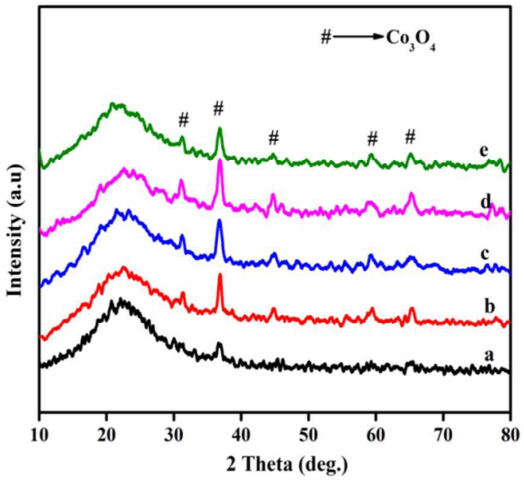

Fig. 2 Wide angle XRD patterns of calcined sample of Co/COK-12 and 5CS-16 catalysts, (a) 3CC-12 (b) 5CC-12 (c) 10CC-12 (d) 20CC-12 (e) 5CS-16

View Article Online
DOI: 10.1039/C8NJ03211D

The wide angle XRD patterns of reduced Co/COK-12 and 5CS-16 catalysts were shown in Fig. 3 The high intense peaks at 2θ value of 44.2° represent (111) metallic phase of cobalt Co (0) with fcc geometry of the space group Fm3m (JCPDF no 150806) [25-26]. A small intense peak at around 2θ value of 42.5˚ indicates the presence CoO crystallites in 5CS-16 catalyst.

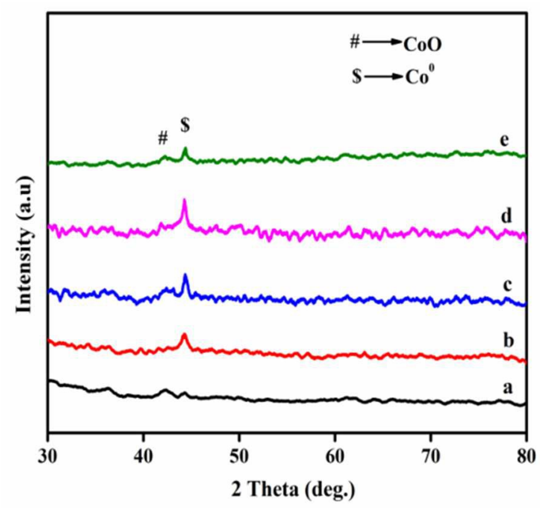

Fig. 3 Wide angle XRD patterns of reduced Co/COK-12 and 5CS-16 catalysts, a) 3CC-12 (b) 5CC-12 (c) 10CC-12 (d) 20CC-12 (e) 5CS-16

The N_2-adsorption desorption isotherms of pristine COK-12, SBA-16 and their supported cobalt catalysts were presented in Fig. 4 & 5. All the COK-12 and Co/COK-12 catalysts exhibit type IV isotherm with H1-type hysteresis loop indicating the ordered mesoporous materials with well ordered hexagonal pores of p6mm geometry [20]. It is a clear indication of intactness of ordered mesoporous structure of parent COK-12 after cobalt deposition. The shift in capillary condensation steps towards lower relative pressure is an indication for partial pore blockage due to the presence of cobalt inside the pores which results decrease in mean pore diameter of Co/COK-12 catalysts [27, 36]. The parent SBA-16 and cobalt deposited SBA-16 catalysts exhibit type IV isotherm with H_2-type hysteresis loop confirming the mesoporous materials with cage like pore structure [23-24]. The pore size distribution patterns of parent, various loaded Co/COK-12 and 5CS-16 catalysts were presented in insert of Fig. 4 & 5. The uni-model pore size distribution is observed in parent and Co/COK-12 catalysts with an average pore diameter of 5-10 nm. The bimodal pore size distribution with an average pore size of 3.5-5 nm for SBA-16 and 5CS-16 catalysts shows the existence of mesoporous nature with cage type pores [28]. The pore size distribution curves (inset of figure 4&5) indicates that majority of pores are concentrated at around 6 nm even though this value is different from the average pore size around 5 nm which is the average value of all the pores present in the sample. In general, after cobalt loading the pore size is smaller than the support, but there are instances in mesoporous silica materials where both the pore size values of support and loaded one are more or less same [29-31]. The textural features of Co/COK-12 and SBA-16 and 5CS-16 catalysts were reported in Table 1. The surface area of the catalysts decreases with the cobalt amount.

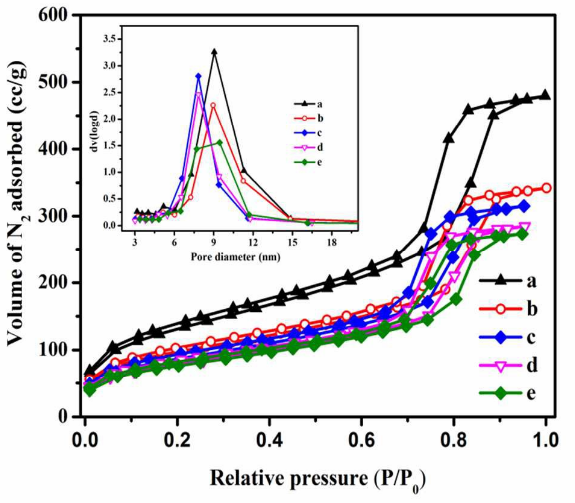

Fig. 4 N_2-adsorption desorption isotherms and pore size distribution patterns of pristine COK-12 and their supported cobalt catalysts calculated from adsorption branch of isotherm, (a) COK-12 (b) 3CC-12 (c) 5CC-12 (d) 10CC-12 (e) 20CC-12.

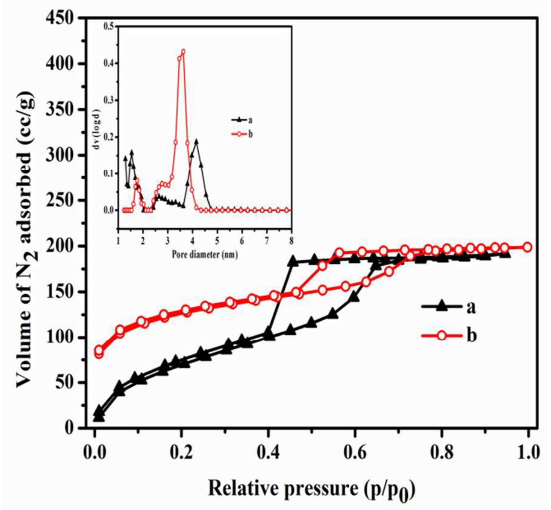

Fig. 5 N_2-adsorption desorption isotherms and pore size distribution patterns of pristine SBA-16 and its supported cobalt catalysts calculated from adsorption branch of isotherm, (a) parent SBA-16 and (b) 5CS-16 catalyst.

SEM and TEM images of COK-12, SBA-16 and their cobalt catalysts were recorded and presented in Fig. 6 &7. SEM images of the pristine COK-12 (6a) and 5CC-12 (6b) catalysts show connected granules type morphology. Both the samples of SBA-16 (6c) and 5CS-16 (6d) catalysts display spheres like morphology with continuous agglomeration [32-35].

View Article Online
DOI: 10.1039/C8NJ03211D

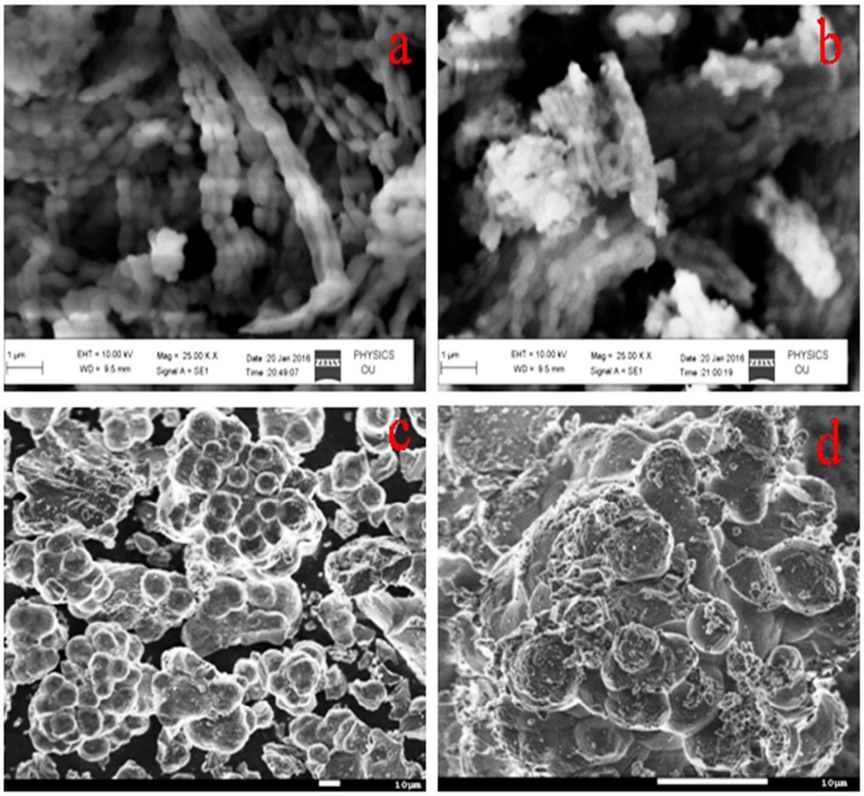

Fig. 6 SEM images of (a) COK-12 (b) 5CC-12 (c) SBA-16 (d) 5CS-16 catalysts.

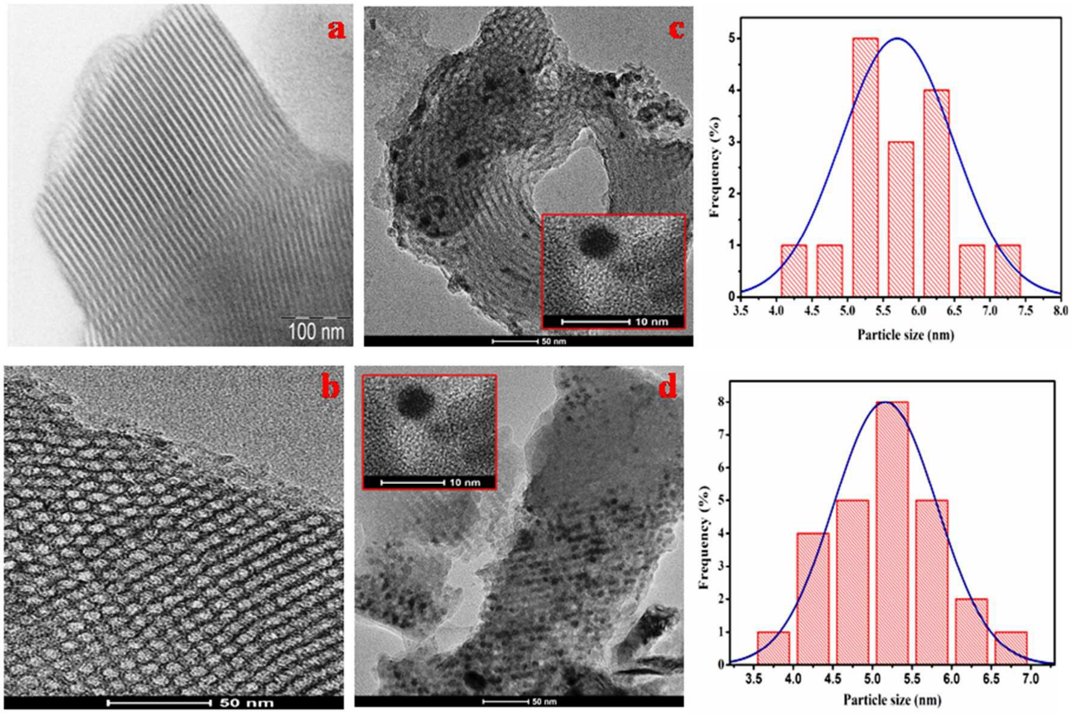

Fig. 7 TEM images of (a) COK-12 (b) SBA-16 (c) 5CC-12 (d) 5CS-16.

View Article Online
DOI: 10.1039/C8NJ03211D

TEM images of COK-12 (Fig.7a) and 5CC-12 (Fig.7c) catalysts shows arrangement of uniform pore channels of honey comb array [34]. TEM images of SBA-16 (Fig.7b) and 5CS-16 (Fig.7d) catalyst clearly show well ordered cage type pores which are typical of 3D-SBA-16 type mesoporous materials [35-36]. TEM image of 5CS-16 shows the presence of cobalt particles in inside of the pore channels. The average particle sizes of cobalt in 5CC-12 and 5CS-16 are 5.6 and 5.1 nm respectively. In both the samples 5CC-12 and 5CS-16 there is a well dispersion of cobalt particles over the mesoporous channels of the support and it can be confirmed that, the mesoporous structure is retained even after cobalt deposition.

Table 1: Physicochemical properties of parent, various loaded Co /COK-12 and 5CS-16 catalysts.

Catalyst	S_{BET}^a (m^2g^{-1})	V_t^b (cc/g)	D^c (nm)	$d_{(100)}^d$ (nm)	a_0^e (nm)	t^f (nm)
COK-12	465	0.48	5.20	8.54	9.87	4.67
3CC-12	345	0.42	4.90	8.66	10.01	5.11
5CC-12	304	0.41	6.01	8.67	10.01	4.00
10CC-12	278	0.34	4.01	8.67	9.93	5.92
20CC-12	220	0.28	4.12	8.97	10.36	6.24
SBA-16	543	0.30	4.42	10.15	11.72	7.3
5CS-16	402	0.28	4.86	10.88	12.56	7.7

a BET Surface area, b Total Pore Volume at relative pressure (P/P_0), c Average Pore size, f pore wall thickness, d Derived from a low angle XRD, e Unit cell length

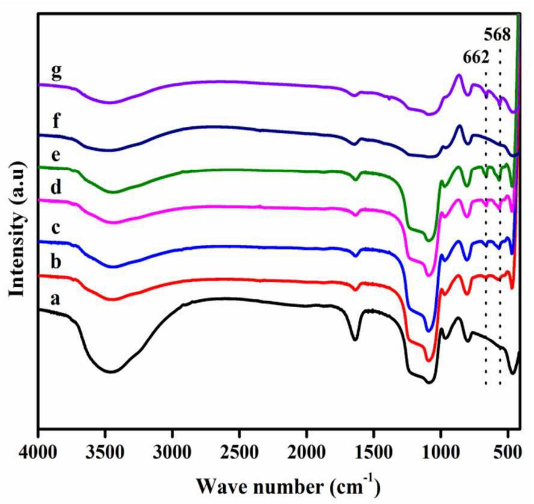

Fig 8 FT-IR spectra of parent, Co/COK-12 and SBA-16 catalysts (a) COK-12 (b) 3CC-12 (c) 5CC-12 (d) 10CC-12 (e) 20CC-12 (f) SBA-16 (g) 5CS-16.

FT-IR spectra of parent, various loaded Co/COK-12 and 5CS-16 catalysts were shown in Fig. 8. The presence of 1087 and 807 cm^{-1} absorption bands correspond to Si-O-Si stretching vibration and another absorption band at 464 cm^{-1} is associated to Si-O-Si bending. The absorption band at 960 cm^{-1} is due to Si-OH or Si-O-Si stretching vibrations. The absorption bands at 662 and 568 cm^{-1} represents the Co-O vibrations in the cobalt oxide lattice [37]. In lower loadings (3 and 5 wt%) the absorption band at around 662 and 568 cm^{-1} are in low intensity due to lower Co loading.

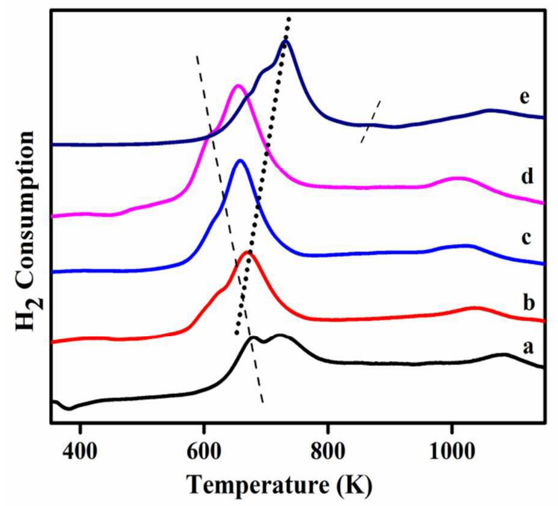

Fig. 9 H_2-TPR profiles of various loaded Co/COK-12 and 5CS-16 catalysts (a) 3CC-12 (b) 5CC-12 (c) 10CC-12 (d) 20CC-12 (e) 5CS-16.

Temperature programmed reduction (H_2-TPR) was performed to evaluate the reducibility of cobalt oxide and metal support interactions and the corresponding profiles were presented in Fig. 9. All the Co/COK-12 and 5CS-16 catalysts show two stage reductions ($Co_3O_4 \rightarrow CoO \rightarrow Co^0$) of cobalt oxide. The first reduction peak at around 600-673 K is due to the reduction of Co_3O_4 ($Co_3O_4 \rightarrow CoO$) and the second reduction peak at around 647-724 K is due to the subsequent reduction of the intermediate CoO ($CoO \rightarrow Co^0$). The reduction temperature gives the relative information about the crystallite sizes of Co_3O_4, the bigger crystallites of Co_3O_4 are easily reduced at lower temperature and the support interactions enhance the reduction temperatures to higher values [38-39]. Hence, the shift in reduction T_{max} of Co/COK-12 catalysts towards lower temperatures is an indicative for the formation of bigger Co_3O_4 species with increase in cobalt loading. In addition to the two reduction peaks, there is another peak at relatively higher temperature (996-1081 K) due to the reduction of Co-silicate like species [40]. From the H_2-TPR profiles, it is interesting to note that, there is a broad reduction profile at slightly higher temperature for 5CS-16 catalyst compared to 5CC-12 catalyst and there is another small reduction peak at 865 K. These results reveal the existence of highly dispersed smaller cobalt oxide particles in 5CS-16 catalyst. To get more insight into the influence of 3D-SBA-16 support on dispersion of cobalt, the TPR profile of 20CC-12 catalyst is compared with 20CS-16 catalyst (Fig. ESI1). It shows that cobalt oxide species present in 20CS-16 catalyst are reduced relatively at higher reduction temperatures than 20CC-12 catalyst. The small cobalt oxide particles which are confined in cage type pores of SBA-16 moves the T_{max} of reduction towards the higher temperature.

View Article Online
DOI: 10.1039/C8NJ03211D

Table 2. H_2 uptake, active metal surface area, Co particle size and cobalt metal dispersion of various loaded Co/COK-12 and 5CS-16 catalysts.

Catalyst	Cobalt loading (wt %)[a]	H_2 uptake (μ moles/g)	Metal surface area [b] (m^2/g cat.)	Metal surface area (m^2/g Co)	Co^0 particle size [c] (nm)	Dispersion (D%) [d]	Co_3O_4 crystallite size (nm)[e]	Co crystallite size (nm)[f]	Co crystallite size (nm)[g]	TOF X10^{-2} (s^{-1}) [h]
3CC-12	2.8	57.56	4.60	164.28	4.10	24.23	8.6	5.6	6.4	2.19
5CC-12	4.72	82.09	6.55	138.77	4.85	20.50	10.4	7.1	7.8	1.64
10CC-12	10.8	129.38	10.32	95.55	7.05	14.12	12.8	10.3	9.6	1.02
20CC-12	19.12	138.05	11.01	57.58	11.70	8.51	15.1	11.7	11.3	0.92
5CS-16	4.84	97.32	7.76	160.33	4.20	23.70	8.2	6.2	6.1	1.23

[a] obtained by ICP-OES, [b, c, d] Obtained from H_2 uptake. [b] Active metal surface area (ASA) = Nm ×S × Am × 6.023×10^{23}; where ASA is in m^2/g of sample; Nm = the number of adsorbed gas molecules (Mole × 10^{-6}/g), S = adsorption stoichiometric, (Co / H_2 =2), Am = the cross-sectional area occupied by each active cobalt surface atom (6.623×10^{-20} m^2), [c] Average Particle size (d) = 10×L×f / ASA×Z; Where L= percentage Cobalt loading, f is a particle Shape correction factor (6 for spherical particles), Z =density of the cobalt metal (8.9 g/cm^3), d is in nm. [d] % Co Dispersion (D) =Nm×S×M / 100 L; Where M is the molecular weight of cobalt (58.9 g), [e] Average crystalline size of Co_3O_4 calculated from the Scherrer equation. [e] Average crystalline size of Co calculated from the Scherrer equation [g] Average crystalline size of Co = ¾ (crystallite size of Co_3O_4) [29]. [h] Reaction conditions: Temperature =488 K, GHSV=387.1 h^{-1}, Pressure =1atm.

TEM image of 5CS-16 catalyst (Fig. 7d) also confirms the location of some cobalt particles in inside of the pores of SBA-16.

The active Co metal surface area, metal dispersion and average particle size of the supported cobalt catalysts was measured by H_2-pulse chemisorption studies and results were reported in Table 2. The amount of H_2 uptake is increased with the amount of cobalt which in turn increases the active metal surface area of the catalysts. The particle size of cobalt increases with the increase in cobalt amount, consequently, the dispersion of the active metal decreases. The order of the active cobalt metal dispersion follows the trend 3CC-12>5CC-12>10CC-12>20CC-12. In support to the results obtained by XRD and H_2-TPR studies, H_2-pulse chemisorption also confirms the relatively higher dispersion and presence of smaller cobalt nanoparticles in SBA-16 than COK-12 supported cobalt catalysts.

Catalytic performance

In order to screen the optimum loading of cobalt, Co/COK-12 catalysts were subjected to the hydrogenation of NB at atmospheric pressure and results were presented in Fig.10. The conversion of NB is increased from 44 to 83% with increase in cobalt amount from 3 to 5 wt%. Upon further increase in the cobalt amount to 10 and 20 wt%, there is a drop in conversion to 64%. However, in all these cases the selectivity to aniline is more or less same. Consequently, the rate of formation of AL increases with the cobalt amount up to 5 wt%, further increase in cobalt amount results down fall. The rate of formation is the activity of all the active sites present in the catalyst. The rate of formation of AL for 5CC-12 catalyst (12.16 μmol.g^{-1}.s^{-1}) is nearly two fold higher than 3CC-12 catalyst (5.95 μmol.g^{-1}.s^{-1}). The low rate of formation of AL over 3CC-12 catalyst is due to insufficient number of active sites. The rate of formation of AL is decreased from 5CC-12 to 20CC-12 catalyst. The order of rate of formation follows the trend as 3CC-12<5CC-12>10CC-12>20CC-12. Turn over frequency (TOF) of Co/COK-12 catalysts is reported in Table 2. TOF can be defined as number of AL molecules formed in one second on one cobalt active site. 3CC-12 catalyst exhibits the highest TOF in the series and 20CC-12 catalyst exhibits the lowest TOF. Even though 3CC-12 catalyst exhibited high TOF value, the yield of AL is less compared to 5CC-12 catalyst. The dispersion of 3CC-12 catalyst is high but the number of active sites is not enough to produce maximum yield of AL. 5CC-12 catalyst with sufficient number of cobalt active species (with Co particle size 4.85 nm Table 2) is able to produce maximum yield of AL. Beyond this, cobalt particle sizes are increased which in turn decreases the yield of AL and TOF. Despite of high dispersion and small cobalt particle size of 5CS-16 catalyst, 5CS-16 catalyst has lower TOF value than 5CC-12 catalyst. The high dispersion and small cobalt particles in cage type pores of 5CS-16 catalyst results formation of other products which promote blocking of active sites. This affects the yield of AL as well as TOF of 5CS-16 catalyst. These results are indicating the significant role of cobalt metal dispersion and particle size on catalytic performance of mesoporous silica supported cobalt catalysts.

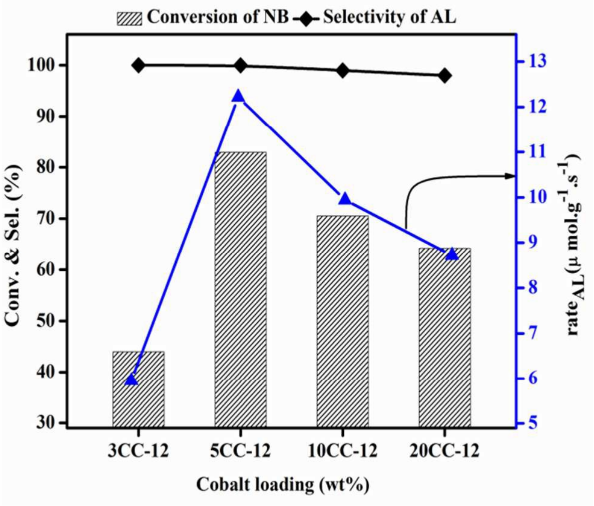

Fig. 10: Effect of cobalt loading on the hydrogenation of NB to AL. Reaction conditions: Temperature =488 K, GHSV=387.1 h^{-1}, Pressure =1atm.

View Article Online
DOI: 10.1039/C8NJ03211D

Fig.11 shows influence of reaction temperature on the hydrogenation of NB over 5CC-12 catalyst. The conversion of NB is decreased with reaction temperature. The complete conversion of NB is achieved at a reaction temperature of 488 K (~ at boiling point of NB). When the reaction temperature is increased from 488 K to 513 K the conversion is decreased to 90 %. Further increase in temperature shows a much more decrease in the conversion of NB. The selectivity to aniline is in the same trend as conversion due to formation of other products. The inverse results in conversion with temperature are due to the exothermic nature of the reaction hydrogenation of NB (~ H= -443 kJ.mol^{-1}). Hence the low temperatures are favourable for the hydrogenation of NB. Moreover, the present reaction temperature (488 K) is the lowest compared to the reported gas phase catalytic systems (Table 4).

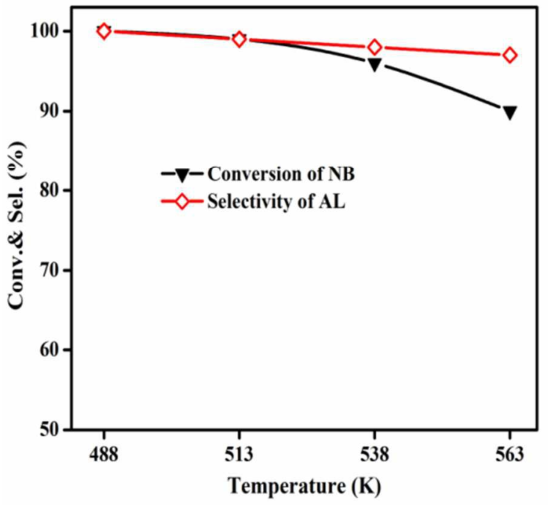

Fig. 11 Effect of temperature on the hydrogenation of NB to AL on 5CC-12 catalyst. Reaction conditions: GHSV=77.41 h^{-1}, Pressure =1atm.

The influence of flow rate of reactant NB on catalytic activity of 5CC-12 catalyst at 488 K was shown in Fig. 12. An optimized flow of H_2 (15 mL.min^{-1}) is used in this study. With increase in GHSV, the conversion of NB is decreased. At a GHSV of 77.41 h^{-1}, complete conversion of NB is obtained with >99 % selectivity to AL.

The lower GHSV offers direct contact between reactant and catalyst surface where the reactant concentration per active site is high, thereby increase the conversion of the reactant. The decline in conversion of NB with increase in space velocity may be due to the reduction of residence time of reactants. It is notable to mention that, the selectivity to AL is always more than 98% irrespective of the space velocity. It reflects the superiority of the 5CC-12 catalyst in selective hydrogenation of NB to AL.

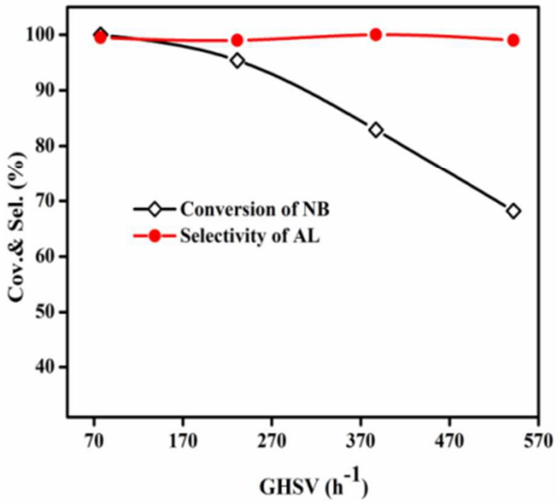

Fig. 12 Effect of reactant flow rate on the hydrogenation of NB to AL on 5CC-12 catalyst. Reaction conditions: Temperature =488K, Catalyst weight = 1 g, pressure = 1 atm.

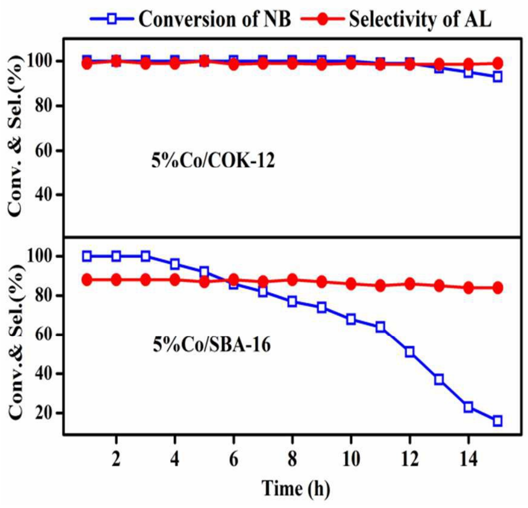

Fig. 13: Time on stream study on the hydrogenation of NB to AL over 5CC-12 and 5CS-16 catalyst. Reaction conditions: Temperature= 488K, GHSV=77.41 h^{-1}, pressure =1atm.

The time on stream study results over 5CC-12 catalyst were shown in Fig.13. It displays the excellence of 5CC-12 catalyst in hydrogenation of NB. The conversion of NB and selectivity to AL is almost constant during 15 h course of reaction. The constant catalytic activity can be ascribed to the stabilization of cobalt nanoparticles over the 2D hexagonal mesoporous pore channels of COK-12 support. As the 2D hexagonal mesoporous silica COK-12 plays a crucial role in dispersion and restricting agglomeration of the cobalt nanoparticles, it is expected that the same results have to obtain with 3D cubic mesoporous silica SBA-16. For this, 5CS-16 catalyst is subjected to the time on stream study under the same experimental conditions and results are presented in Fig.13. Interestingly, the 5CS-16 catalyst experiences continuous loss in the conversion of NB from 100 % to 15 % at the end of 15th hour.

View Article Online
DOI: 10.1039/C8NJ03211D

The discrepancy in catalytic performance of mesoporous silica supported cobalt catalysts can be explained by assessing the products distribution and the characterization of spent catalyst. The XRD patterns of both 5CC-12 and 5CS-16 spent catalysts were collected and presented in Fig.14. Comparing the fresh and spent XRD profiles of 5CC-12 and 5CS-16 catalysts, there are no structural changes occurred in both the catalysts after the time on stream study. The fresh and spent catalysts of 5CC-12 and 5CS-16 are characterized by XRD and found that there is no significant change in the average crystallite sizes cobalt, which indicates the dispersion of cobalt over mesoporous silica is resistant to the agglomeration of cobalt particles. It means the decrease in catalytic performance doesn't relate to either agglomeration of cobalt nanoparticles or destruction of mesoporous nature of the catalysts.

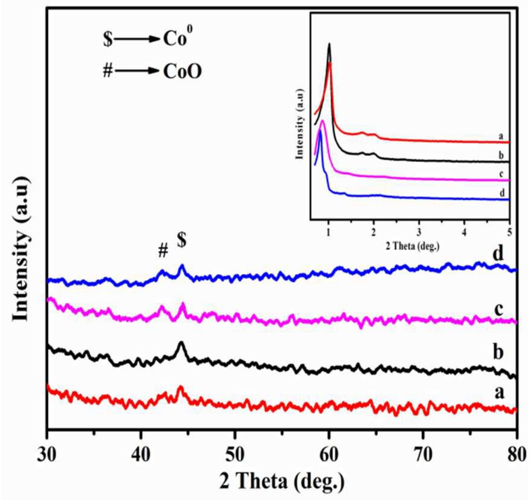

Fig. 14 The low (Insert fig.14) and wide angle XRD patterns of fresh and spent 5CC-12 and 5CS-16 catalysts, (a) U5CC-12 (b) 5CC-12 (c) U5CS-16 (d) 5CS-16.

The water molecules released during the hydrogenation of NB to AL don't influence the catalytic performance of the mesoporous silica supported catalysts due to water resistant behavior of the mesoporous silica [22]. The drastic variation in the catalytic activity of 5CS-16 catalyst can be explained in terms of deposition coke (carbonaceous species) over the catalyst surface. To get more insight on this, the products formed over 5CC-12 and 5CS-15 were analyzed. A diverse product distribution is noticed with 5CS-16 catalyst showing products like phenyl-cyclohexyl amine, Cyclohexanone which are formed only after the formation of AL (as shown in Scheme 1). The formation of these products exclusively with 5CS-16 catalyst suggests that there are intense hydrogenation reactions catalyzed by smaller cobalt nanoparticles confined within interconnected network cage type pores of 3D cubic SBA-16. The presence of smaller cobalt nanoparticles inside the pores of 3D cubic SBA-16 can be evidenced by the H_2-TPR. In addition to this, the surface coverage and surface density of 5CC-12 catalyst is higher than 5CS-16 catalyst. The high surface coverage (2.2 %) and surface density (54.0 %) of 5CC-12 catalyst indicates the presence of the most of Co particles located outside of the pores of support COK-12. The low surface coverage (1.9 %) and surface density (48.4%) of 5CS-16 catalyst indicates the location of Co particles either outside as well as inside the pore network of support SBA-16. The interconnectivity of pores in 5CS-16 catalyst allows the molecules to stay with cobalt nanoparticles for longer residence times consequently the molecules undergo successive reactions. Owing to these reactions, selectivity to AL is decreased in 5CS-16 compared to 5CC-12 catalyst and also generates coke formation via condensed products over the active sites. As long as this process continues, accumulation of coke over the active sites continuously occurs thereby results dwindling in conversion of NB. The formation of coke over the active sites can be confirmed by means of H_2-TPR, TGA (Thermo Gravimetric Analysis) and CHNS elemental analysis of the spent catalysts. TGA profiles of both U5CC-12 and U5CS-16 were displayed in Fig.15. It can be observed that, there is high weight loss in the U5CS-16 catalyst relative to the U5CC-12 catalyst. It indicates that more amounts of carbonaceous species have been deposited over U5CS-16 compared to U5CC-12 catalyst. 5CS-16 catalyst suffers from intense hydrogenation reactions which produce a diverse coke compared to coke produced in 5CC-12 catalyst. Hence, TGA thermogram of U5CS-16 catalyst shows weight loss at relatively higher temperature than U5CC-12 catalyst. N_2-physisorption results of spent and regenerated 5CC-12 and 5CS-16 catalysts were presented in Fig.ESI 2&3 and the textural features these catalysts presented in table ESI 1. All the catalysts show the retention of mesoporous structure by exhibiting corresponding isotherms (Type IV isotherm with H1-(5CC-12) and H2-hysteresis (5CS-16) loops). It supports the XRD results that there is no structural collapse in 5CC-12 and 5CS-16 catalysts after the reaction. The surface areas of fresh, spent and regenerated 5CC-12 catalysts are 304, 233 and 289 m^2/g respectively. The surface area of 5CC-12 catalyst is decreased due to the deposition of coke during the reaction which is reflected in surface area and total pore volume of spent 5CC-12 catalyst. After calcination (at 873 K for 5 h) in air flow to remove the coke present in spent catalyst, regenerated 5CC-12 catalyst recovers its surface area to 289 m^2/g. The surface areas of fresh, spent and regenerated 5CS-16 catalysts are 402, 76 and 390 m^2/g respectively. The surface area and pore volume of spent 5CS-16 catalyst is drastically diminished due to severe deposition of coke which promotes pore blocking. After regeneration, 5CS-16 catalyst regains its surface area from 76 to 390 m^2/g and pore volume from 0.08 to 0.29 cc/g. It could be observed that the decrease in surface areas of spent catalysts is relatively more in 5CS-16 than 5CC-12 catalyst. These results illustrate that the catalyst deactivation in 5CS-16 is due to the accumulation of coke over the active sites which causes pore blocking. This pore blocking is observed to be more in 5CS-16 with cage type interconnected pores than in 5CC-12 catalyst.

View Article Online
DOI: 10.1039/C8NJ03211D

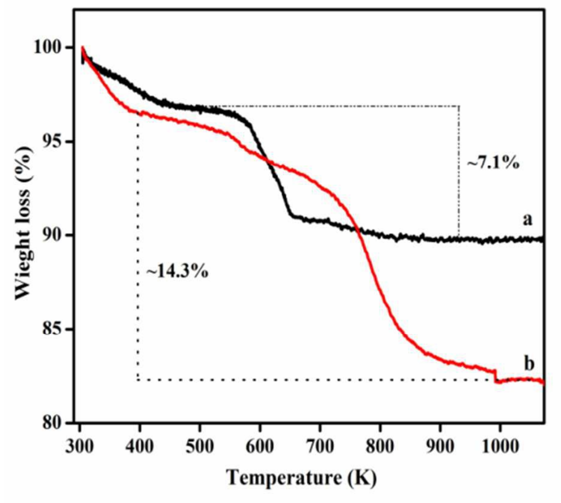

Fig. 15 TGA thermograms of a) U5CC-12, (b) U5CS-16

CHNS elemental analysis of U5CC-12 and U5CS-16 catalysts was performed and the results were presented in Table 3. The obtained amount of coke deposited on spent catalysts by both CHNS elemental analysis and TGA is almost the same. The rate of carbon formation (~0.9 mmoles.g^{-1}.h^{-1}) is more in the case of U5CC-12 catalyst which means the formation of condensed products is more over 3D-cubic pores of SBA-16.

Table 3: TGA and CHNS elemental analysis data of 5CC-12 and 5CS-16 spent catalysts after 15h Time on stream.

Catalyst	Carbon (Wt %)		Rate of carbon formation (m moles.g^{-1}.h^{-1})	
	CHNS	TGA	CHNS	TGA
U5CC-12	6.7	7.1	0.4	0.42
U5CS-16	13.9	14.3	0.9	0.93

In general, carbonaceous species present over the catalyst surface can be identified by performing H_2-TPR study where the carbonaceous species hydrogenated and evolved as CH_x showing a negative signal in the corresponding TPR profile [41]. Fig.16. shows H_2-TPR profiles of both the spent catalysts. Both the U5CC-12 and U5CS-16 catalysts exhibit a broad negative peak in the temperature range of 700-940 K. The negative peak in U5CS-16 catalyst is shifts to higher temperature due to the hydrogenation of carbonaceous species present in the cage type pores of SBA-16. The formation of unavoidable coke causes severe catalytic deactivation of 5CS-16 catalyst in the hydrogenation of NB. The catalytic activity of 3D-SBA-16 with pore sizes lower (5CS-16 (1)) and higher pore sizes (5CS-16 (2)) than 4.86 nm have been studied and the results were presented in supporting information (Fig.ESI 4&5). These two catalysts show a similar catalytic activity during the time on stream study irrespective of the pore size of SBA-16.

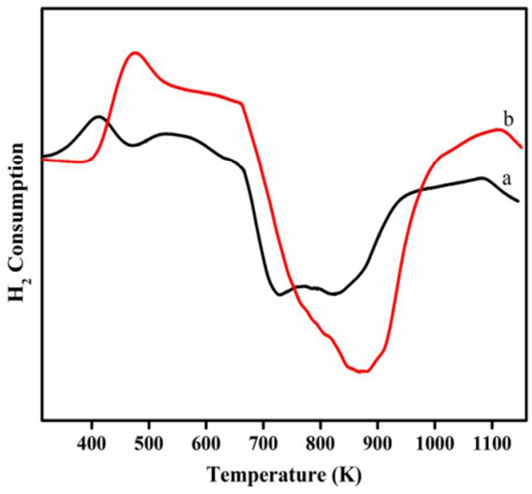

Fig. 16 H_2-TPR profiles of (a) U5CC-12, (b) U5CS-16.

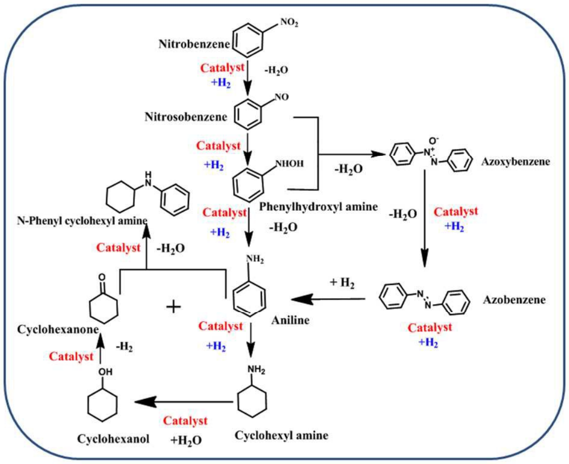

Scheme 1. Plausible reaction pathway for the hydrogenation of nitrobenzene on Co/COK-12 and Co/SBA-16 catalysts.

The catalytic performance of the mesoporous silica (2D-hexagonal COK-12 and 3D- cubic SBA-16) supported cobalt catalysts is compared with reported catalytic systems and tabulated in Table 4. Cheng et al. prepared organic imine groups functionalized SBA-15 support for the dispersion of Pt-Pd bimetallic nanoparticles and applied for the hydrogenation of NB in batch process [15]. However, the complexity in the functionalized SBA-15 catalyst preparation limits its practical application. Huiping et al. developed spherical like Pt-MCM-41 catalyst and compared its catalytic performance with conventional prepared Pt/MCM-41 catalyst [16]. It is reported that, spherical like Pt-MCM-41 is more active than Pt/MCM-41 catalyst for hydrogenation of NB in batch process under 5 bar H_2 pressure. Both these processes are associated with the use of noble metals and need of separation of solvent and catalyst from the product. Sangeetha et al. examined Pd/HT catalysts for hydrogenation of NB in continuous process at 498 K [7]. Pd/HT catalyst showed drastic decrease in both conversion

View Article Online
DOI: 10.1039/C8NJ03211D

and selectivity after 3 h during the time-on-stream study. It is found that, the water molecules released during the hydrogenation of NB alter the phase of HT. Ru/SBA-15, Au-Co/SBA-15, Ru/C and Cu/MgO catalysts were reported for hydrogenation of NB in continuous process. The catalyst stability during time-on-stream is a prerequisite parameter for evaluation of the catalytic system. There is no information about the stability of these catalysts during time-on-stream studies [9, 17, 10, and 12]. The pre-carbon coating over the supports helps to maintain the catalytic performance of Ni/C-Al_2O_3 and Co/C-SiO_2 catalysts in hydrogenation of NB [11c, 25]. Co/SiO_2 catalyst without carbon coating is deactivating during time-on-stream study. There is a need for the surface modification of support SiO_2 by carbon coating. It is tedious process and amount of carbon to be deposited is also important for catalytic performance. However the present Co/COK-12 catalyst doesn't need any modification of support COK-12 and it is stable under reaction conditions. Unlike reported catalytic systems, the present catalytic system offers a non-noble metal Co based catalyst for hydrogenation of NB at 488 K under atmospheric pressure in continuous process. The reaction temperature used in this reaction is lower than the reported catalytic systems in continuous mode. The present catalytic system offers no need of solvent and excluded from the separation steps. Most of the reported catalytic systems in continuous process are deactivated due to the release of water molecules during NB hydrogenation. The hydrophobic nature of mesoporous silica and uniform distribution of cobalt nanoparticles assist the Co/COK-12 catalyst to yield better results. The stable catalytic activity and selectivity of Co/COK-12 during time-on-stream study demonstrates its excellence in hydrogenation of NB in continuous process at atmospheric pressure.

Conclusions

The mesoporous silica (2D-hexagonal COK-12 and 3D- cubic SBA-16) supported cobalt catalysts are found to be active and selective in the gas phase hydrogenation of nitrobenzene at atmospheric H_2 pressure. The mesoporous nature of silica supports is helpful in stabilization of cobalt nanoparticles. For Co/COK-12 catalysts, the catalytic performance is strongly influenced by dispersion and particle size of cobalt nanoparticles. In the case of SBA-16 supported cobalt catalyst the support architecture plays a decisive role in directing the catalytic performance. Compared to the 2D-hexagonal COK-12 supported catalyst, 3D-cubic SBA-16 with interconnected pores enables the reactant molecules to stay for longer residence times with the cobalt nanoparticles. Subsequently, molecules tend to participate in successive reactions results condensed products and create coke formation during the course of reaction. 3D-cubic SBA-16 with interconnected pores is not a preferable support for hydrogenation of nitrobenzene under these reaction conditions due to its rapid deactivation. 2D-hexagonal COK-12 supported cobalt catalyst offers hexagonal pore channels to felicitate the hydrogenation of nitrobenzene and is stable during 15 h time on stream study with complete conversion of nitrobenzene and >99% selectivity to aniline.

Conflicts of interest

There are no conflicts to declare.

Acknowledgements

KM and ESS, are grateful to University Grants Commission (UGC), New Delhi, India for the award of Fellowship.

Table 4: Comparison of nitrobenzene hydrogenation activities of 5 wt% Co/COK-12 and 5wt% Co/SBA-16 catalyst with the reported catalysts in continuation process at atmospheric pressure.

Catalyst	Operating Conditions		Nitrobenzene Conversion (%)	Aniline Selectivity (%)	Reference
	Temperature (K)	H_2/NB			
0.5 wt% Pd/HT	498	4	97	100	[7]
4.5 wt% Ru/SBA-15	548	4	94	100	[9]
4.5 wt% Ru/C	548	4	90	100	[10]
5wt%Ni/C-Al_2O_3	498	4	99	100	[11c]
25wt%Cu/MgO	553	4	94	100	[12]
Pt-Pd/organo-SBA-15	333 (Batch process)	-	100	>99	[15]
Pt-MCM-41	303 (Batch process)	-	91	~94	[16]
Au-Co/SBA-15	473	-	99	100	[17]
5 Wt% Co/ C-SiO_2	498	4	100	> 99	[25]
5wt%Co/COK-12	488	4	100	> 99	Present study
5wt%Co/SBA-16	488	4	100	~ 88	

DOI: 10.1039/C8NJ03211D

References

1 Wiley. (2006) Ullmann's encyclopedia of industrial chemistry (7th Ed.). New York, NY: Wiley.

2 B. Saha, D. Sudipta and D. Saikat, Critical Reviews in Environmental Science and Technology, 2013, **43**, 84.

3 A. S. Travis and Z. Rapp port, The Chemistry of Anilines, John Wiley and Sons, (2007) p. 715.

4 F. Zhao, Y. Ikushima and M. Arai, J .Catal. 2004, **224**, 479.

5 L. Chun-Hua, Y. Zhen-Xing, Y. Ke-Fu, J. Sheng-fu and J. Liang, J. Mol. Catal. A: Chem. 2005, **226**, 101.

6 Y. Xibin, W. Minghui and L. Hexing, Appl. Catal. A: Gen. 2000, **202**, 17.

7 P. Sangeetha, P. Seetharamulu, K. Shanthi, S. Narayanan and K. S. Rama Rao, J. Mol. Catal. A: Chem., 2007, **273**, 244,

8 N. Bouchenafa-Saib, P. Grange, P. Verhasselt, F. Addoun and V. Dubois, Appl. Catal. A: Gen. 2005, **286**, 167.

9 K. V. R. Chary and Ch. S. Srikanth, Catal. Lett 2009, **128**, 164.

10 Ch. S. Srikanth, V. Pavan Kumar, B. Viswanadham, A. Srikanth and K. V. R. Chary, J. Nanosci and Nanotech, 2014, **14**, 1.

11 V. Mohan, C. V. Pramod, M. Suresh, K. H. P. Reddy, B. D. Raju and K. S. Rama Rao. Catal. comm. 2012, **18**, 89; V. Mohan, V. Venkateshwarlu, P. Ramudu, M. Ashok Raju, B. David Raju and K. S Rama Rao. Appl. Petrochem. Res. 2016, **6**, 15; V.Venkateshwarlu, V. Mohan, M. Venkata Rao, P. Nagaiah, B. D. Raju and K. S.Rama Rao, Catal. Comm. 2016, **86**, 1.

12 K. H. P. Reddy, R. Rahul, S. S. V. Reddy, B. D. Raju and K. S. Rama Rao, Catal. Comm. 2009, **10**, 879.

13 Y. Sakamoto, M. Kaneda, O. Terasaki, D. Y. Zhao, J. M. Kim, G. Stucky, H. J. Shin and R. Ryoo, Nature 2000, **408**, 449.

14 G. Saidulu, E. S. Sankar, M. R. Kumar, K. S. Rama Rao and B. D. Raju, Catal. Sci. Technol., 2014, **4**, 1813.

15 Ch. Liu, R. Tan, N. Yu, D. Yin, Microporous and Mesoporous Materials. 2010, **131,** 162.

16 H. Liu, G. Lu, Y. Guo, Y. Wang, Y. Guo, J. Colloid and Interface Science. 2010, **346**, 486.

17 S. Viswanathan, B. Narayanan, Z. Yaakob, P. Periyat, S. Padikkaparambil, J. Porous Mater 2014, **21**, 251.

18 J. Taghavimoghaddam, G. P. Knowles and A. L. Chaffee, J. Mol. Catal. A: Chem., 2012, **358**, 79.

19 M. Audemar, C. Carmen Ciotonea, K. D. O Vigier, S. Royer, A. Ungureanu, B. Dragoi, E. Dumitriu and F. Jerome, Chem. Sus. Chem. 2015, **8**, 1885.

20 R. J. Jammaer, A. Aerts, J. D .Haen, J. W. Seo, J. A. Martens, J. Mater. Chem., 2009, **9**, 8290.

21 R. M. Grudzien, B. E. Graicka and M. Jaroniec, J. Mater. Chem., 2006, **16**, 819.

22 L. Wang, M. Zhang, M. Zhang, G. Sha and C. Liang, Energy Fuels, 2013, **27**, 2209.

23 E. Siva Sankar, G. V. Ramesh Babu ,Ch. Raji Reddy , B. David Raju and K. S. Rama Rao , J. Mol. Catal. A: Chem. 2017, **426**, 30.

24 E. Siva Sankar, K. Saidulu Reddy, Y. Jyothi, B. David Raju and K. S. Rama Rao, Catal. Lett. 2017, **147**, 2807.

25 K. Murali, E. Siva Sankar, M .Ashok Raju, M. Venkata Rao, B. David Raju and K. S. Rama Rao, Chemistry Select, 2017, **2**, 5716.

26 K. Murali, E. Siva Sankar, G. V. Ramesh Babu, Ch. Raji Reddy, B. David Raju and K.S. Rama Rao. J. Ind. Chem. Eng. 2018, **61**, 227.

27 A. Martinez, C. Lopez, F. Marquez, and I. Diaz, J. Catal. 2003, **220**, 486.

28 Y. Kim, X. Guo and G. Kim, Chem. Commun. 2009, **28**, 4296.

29 Y. Zhao, Y. Zhang, J. Chen, J. Li, K. Liew and M. R. B. Nordin, Chem, Cat, Chem. 2012, **4**, 265.

30 B. David Raju, K. Choi, J. Lee, D. Han, S. Park, Cat. Comm. 2007, **8**, 43.

31 Y. Chen, Y. Cao, Y. Suo, G. Zheng, X. Guan, X. Zheng, J. the Taiwan Institute of Chemical Engineers, 2015, **51** 186.

32 W. J. J. Stevens, M. Mertens, S. Mullens, I. Thijs, G.V. Tendeloo, P. Cool, E. F. Vansant, Microporous Mesoporous Mater. 2006, **93**, 119.

33 A. B. Mohamed, J. M. Cordoba and M. Oden, Microporous Mesoporous Mater. 2010, **129**, 106.

34 E. Siva Sankar G. V. Ramesh Babu, K. Murali, B. David Raju and K. S. Rama Rao, RSC Adv. 2016, **6**, 20230.

35 O.C. Gobin, Y. Wan, D. Zhao, F. Kleitz and S. Kaliaguine, J. Phys. Chem. C, 2007, **111**, 3053.

36 Y. K. Hwang, J. S. Chang, Y. U. Kwon and S. E. Park, Microporous Mesoporous Mater. 2004, **68**, 21.

37 L. Ji, J. Lin and H. C. Zeng, J. Phys. Chem. B, 2000, **104**, 1783.

38 P. Arnoldy and J. A. Moulijn, J. Catal. 1985, **93**, 38.

39 B. Viswanathan and R. Gopalakrishnan, J. Catal., 1986, **99** 342.

40 H. Li, S. Wang, F. Ling and J. Li, J. Mol. Catal. A, 2006, **244**, 33-40.

41 S. Chandra Shekar, J. Krishna Murthy, P. Kanta Rao, K. S. Rama Rao, J. Mol. Catal. A: Chem, 2003, **191**, 45.

View Article Online
DOI: 10.1039/C8NJ03211D

Graphical abstract

Mesoporous silica supported cobalt catalysts for gas phase hydrogenation of Nitrobenzene: Role of pore structure on stable catalytic performance

Murali Kondeboina,[a] Siva Sankar Enumula,*[a] Venkata Ramesh Babu Gurram,[a] Jyothi Yadagiri,[a] David Raju Burri,[a] Seetha Rama Rao Kamaraju*[a]

Catalysis and Fine Chemicals Division, CSIR-Indian Institute of Chemical Technology, Hyderabad, India-500 007, E-mail: ksramaraoiict@gmail.com Fax: +91-40-27160921, Tel: +91-40-27193163.

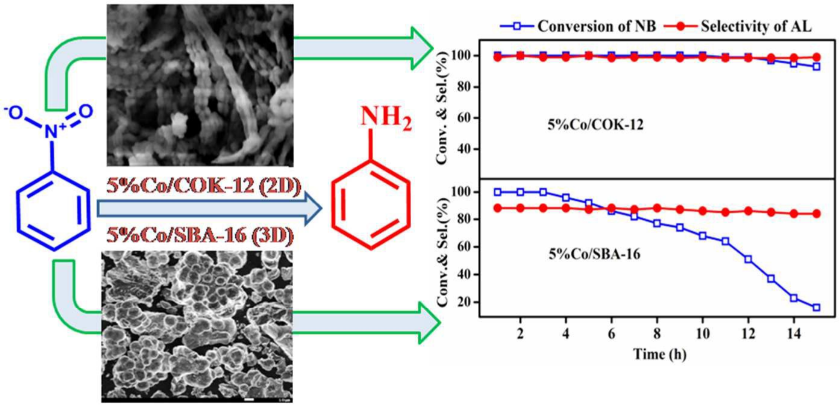

Mesoporous silica supported cobalt catalysts (Co/COK-12 and Co/SBA-16) are active for hydrogenation of nitrobenzene to aniline in continuation process at atmospheric pressure. The support pore architecture is decisive to maintain stable catalytic performance